nature communications

Article

https://doi.org/10.1038/s41467-025-65926-2

Bidentate mixed-ligand strategy in dinuclear gold photoredox catalysis

Received: 11 August 2025

Accepted: 24 October 2025

Published online: 09 December 2025

Check for updates

Qing-Yun Fang[1], Siyu Xia[1], Tingrui Li[1], Yuxi Gao[1], Xiaopeng Wu[1,2] ✉, Weipeng Li[1] ✉, Jie Han[1], Chengjian Zhu[1] ✉ & Jin Xie[1,3] ✉

Dinuclear metal complexes have fascinated researchers for decades owing to their unique metal-metal interactions and electronic synergies, which often lead to unconventional reactivity and exceptional catalytic performance. Despite recent efforts in dinuclear gold photoredox catalysis, limited accessibility of structurally diverse architectures has hindered an in-depth understanding of the Au-Au cooperativity, ligand effect, and structure-property relationships. Here, we report a bidentate mixed-ligand strategy for the modular synthesis of unsymmetrical, tricoordinate dinuclear gold complexes featuring both bisphosphine (P^P) and bipyridine (N^N) ligands. Interestingly, photophysical and computational studies reveal that ligand-to-ligand charge transfer (LLCT), coupled with Au-Au interactions, drives excited-state charge redistribution, enabling inner-sphere single-electron transfer (ISET) for inert C–Br bond activation. These complexes can catalyze three-component carbonylative amidation of unactivated alkyl bromides with amines and CO (balloon) under mild conditions, affording amide products (64 examples) in up to 96% yield.

Photoinduced transition-metal catalysis has established a powerful paradigm for achieving challenging organic transformations[1–3]. Recently, photoexcited gold catalysts have attracted significant attention owing to their unique catalytic performance by integration of exceptional carbophilicity, tunable redox behavior, and rich photophysical properties[4–9]. In particular, dinuclear gold complexes have fundamentally expanded catalytic possibilities beyond mononuclear systems. Recent studies have revealed that the synergistic Au-Au interactions can dramatically reduce activation barriers through cooperative bond cleavage and formation processes[10–14]. However, the limited synthetic accessibility of structurally diverse dinuclear gold complexes has severely hindered the advances in their photocatalytic applications, as most reported systems are based on a single class of symmetric ligands (Fig. 1a)[15–21].

As our continual interests in bimetallic chemistry[10–14,22–30], we sought to employ two different kinds of bidentate ligands (P^P and N^N frameworks) to precisely modulate the coordination microenvironments and structural diversity of dinuclear gold complexes, thereby broadening their synthetic landscape (Fig. 1b). By pairing σ-donating bisphosphine and π-conjugated bidentate nitrogen ligands, the resulting complexes enable ligand-to-ligand charge transfer[31,32] (LLCT) to channel photoexcitation energy toward substrate activation. In the case of organic halides, the Au-Au interaction serves as both a structural anchor and electronic conduit. This synergistic interaction, combined with LLCT, stabilizes a polarized excited state and lowers the C-X bond activation barrier through back-donation (Fig. 1c), ultimately producing open-shell radicals via inner-sphere single-electron transfer (ISET)[33–35]. Consequently, these alkyl radicals can further capture CO to undergo mild carbonylative amidation[36–40] with amines, enabled by dinuclear gold photoredox catalysis (Fig. 1d). Notably, homogeneous gold-catalyzed carbonylation reactions are generally challenging due to the poor compatibility of CO within redox catalytic

[1]State Key Laboratory of Coordination Chemistry, Jiangsu Key Laboratory of Advanced Organic Materials, Chemistry and Biomedicine Innovation Center (ChemBIC), School of Chemistry and Chemical Engineering, Nanjing University, Nanjing, China. [2]Jiangsu Key Laboratory for Recognition and Remediation of Emerging Pollutants in Taihu Basin, School of Environmental Science and Engineering, Wuxi University, Wuxi, China. [3]State Key Laboratory of Natural Medicines, China Pharmaceutical University, Nanjing, China. ✉e-mail: wuxp@cwxu.edu.cn; lwp1989@nju.edu.cn; cjzhu@nju.edu.cn; xie@nju.edu.cn

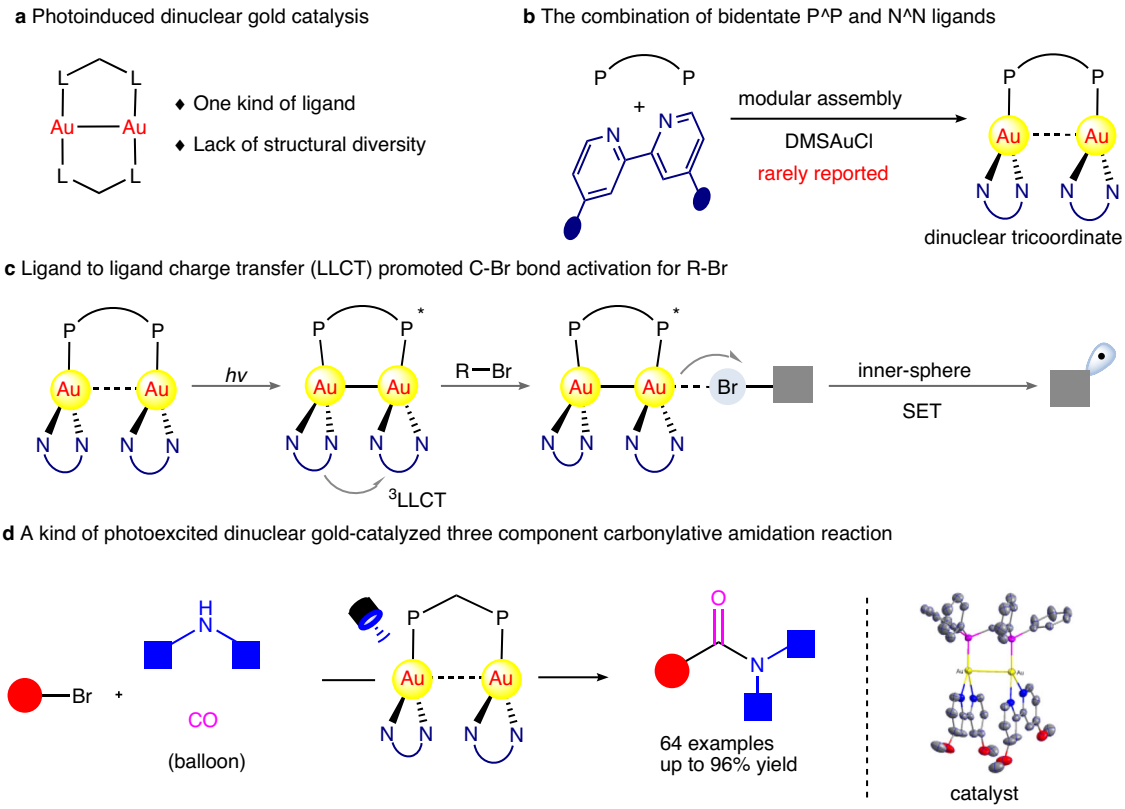

Fig. 1 | Design and catalytic applications of dinuclear tricoordinate gold complexes. a Photoinduced dinuclear gold catalysis. **b** The combination of bidentate P^P and N^N ligands. **c** Ligand to ligand charge transfer (LLCT) promoted C-Br bond activation for R-Br. **d** A kind of phtoexcited dinuclear gold-catalyzed three component carbonylative amidation reaction.

systems for the formation of Au-carbonyl complex[41–45]. A limitation that has recently been addressed by Patil and co-workers applies only in the CO insertion of aryl/vinyl iodides assisted by chelated ligands[46].

Here, we report a method for the synthesis of dinuclear gold complexes through a mixed-ligand strategy incorporating both P^P- and N^N-bidentate ligands. A comprehensive investigation of their photophysical properties reveals the critical role of LLCT and Au-Au interactions in modulating catalytic performance. The LLCT process in the photoexcited state acts as a key driving force for ISET, effectively cleaving unactivated C-Br bonds through back-donation. These complexes exhibit excellent catalytic efficiency in carbonylative amidation of alkyl halides, with broad functional group tolerance and a wide substrate scope. Mechanistic studies uncover a dual ISET/outer-sphere electron transfer (OSET) pathway involving both radical initiation and 4-dimethylaminopyridine (DMAP)-assisted acyl pyridinium formation.

Results and discussion

Design of mixed ligand dinuclear gold complexes

To synthesize dinuclear gold complexes based on a mixed-ligand strategy, we employed complementary P^P- and N^N-type bidentate ligands. Nitrogen-based bidentate ligands, such as bipyridine (bpy) and 1,10-phenanthroline (phen), with their distinctive π-accepting character and rigid chelating geometry[47–50], are well-suited to modulate the electronic excitation properties of dinuclear gold complexes, and allow fine-tuning of catalytic performance through functional group modification[51,52]. Coordination of P^P-$(AuCl)_2$ complexes with bipyridines bearing either electron-withdrawing or electron-donating groups afforded mixed-ligand dinuclear gold-complexes (**4**–**12**) in good yields (64–92%) (Fig. 2). Replacing bis(diphenylphosphino) methane (dppm) with P^N^P-type phosphines or 1,3-bis(diphenylphosphino)propane (dppp) gave complexes **13** and **14** in slightly reduced yields (62% and 68%, respectively). A series of additional gold complexes (**15**–**19**) incorporating various counterions were also prepared in consistently good yields. Single-crystal X-ray diffraction analyses of representative complexes (**4**, **7**, **9** and **12**) revealed Au-Au distances ranging from 3.0 to 3.2 Å, suggesting the presence of significant aurophilic interactions. It is noted that the distance between gold and nitrogen is unequal, and this unsymmetric coordination of the *N,N*-chelates to gold reflects a clear manifestation of the antichelate effect[53,54].

Photophysical properties study

Subsequent investigation of the photophysical properties of gold complex **4** revealed significant solvent-dependent modulation. UV-vis absorption spectroscopy demonstrated a pronounced bathochromic shift in both absorption and emission spectra when the solvent was changed from dichloromethane (DCM) to dimethyl sulfoxide (DMSO) (Fig. 3a, b). This strong solvatochromic effect indicates the influence of solvent environment on the excited-state properties of the gold complexes. Time-dependent density functional theory (TD-DFT) simulations successfully reproduced the experimental absorption spectrum of complex **4** in DMSO. Notably, a prolonged fluorescence lifetime of 1.8 μs was observed in DMSO, providing valuable insight into the long-lived excited state of the complex and underscoring its potential applications in light-driven applications.

To elucidate the charge transfer mechanisms of these dinuclear gold complexes, we performed electron-hole analyses[55–57] on representative examples, as illustrated in Fig. 3c. For clarity and comparability, each complex was partitioned into four structural fragments:

https://doi.org/10.1038/s41467-025-65926-2

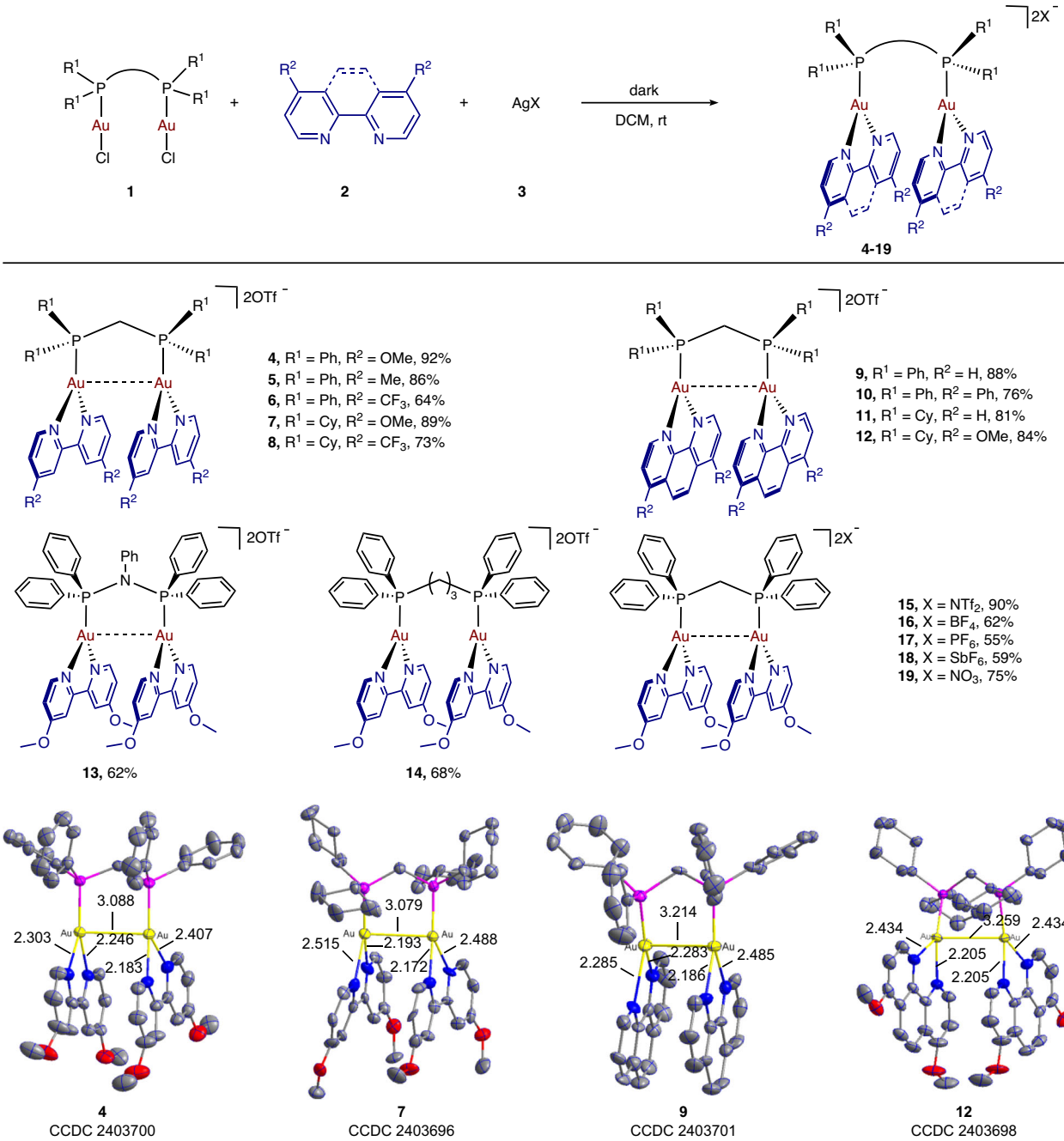

Fig. 2 | Mixed ligands in dinuclear gold complexes. Reaction conditions: **1** (1.0 equiv.), **2** (2.0 equiv.), **3** (2.0 equiv.), ambient temperature, 12 h. The trifluoromethanesulfonate anion is omitted in the single-crystal structure diagrams.

the dinuclear gold core (#1), the phosphine ligand (#2), the counterion (#3), and the nitrogen ligand (#4) (see Supplementary Information for details). Our objective was to quantify the contribution of each fragment to the excitation process and thereby elucidate the underlying charge transfer modes. The computational results demonstrated a high degree of complexity and diversity in the electron distribution across the excited states. In the singlet excited state (S_1), all examined complexes consistently exhibited a predominant charge transfer character from the metal center (M) and phosphine ligand (P) to the nitrogen ligand (N), namely $ML_P(L_N)CT$. This consistency suggests specific electronic arrangements and interaction patterns between the phosphine and nitrogen ligands in the complexes, shaped by their alignment with the relative frontier orbital energies of the metal center.

However, upon transition to the triplet excited state (T_1), the diversity in electron distribution becomes more diversified. Taking the T_1 state of complex **4** as an example, it primarily exhibits LLCT characteristics. This indicates that in the triplet state, excitation-induced electron redistribution is no longer restricted to a single mode. Such changes are likely attributed to alterations in the electron spin configuration and orbital reordering in the triplet state, which significantly modulate the electron distribution and excited-state electronic structure and in turn have a significant impact on the electron transfer modes. Collectively, these findings highlight that the photophysical properties of these mixed-ligand dinuclear gold complexes are governed not only by their ground-state electronic structures, but also critically depend on the excited-state charge transfer nature.

https://doi.org/10.1038/s41467-025-65926-2

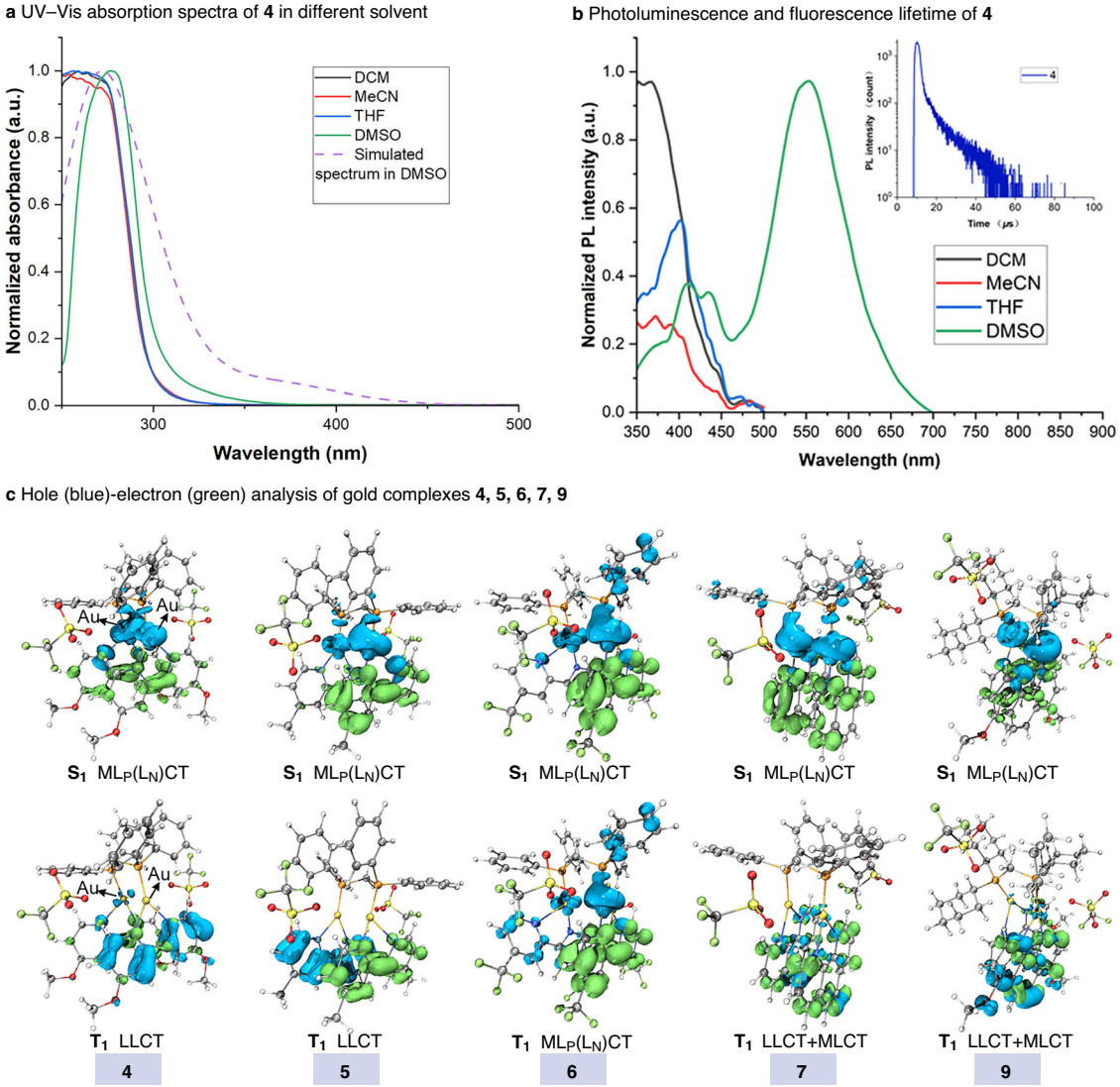

Fig. 3 | Photophysical characterization of gold complexes. a UV-Vis absorption spectra of **4** in different solvents. **b** Photoluminescence and fluorescence lifetime of **4**. **c** Hole (blue)-electron (green) analysis of gold complexes **4**, **5**, **6**, **7** at the level of TDDFT: PBE0(D3)/DKH2/DKH-def2-TZVP (nonmetals)/SARC-DKH-TZVP (metals). Isosurfaces for hole-electron of selected structures are shown (isovalue = 0.002).

Photochemical reaction discovery

Building upon the fundamental understanding of the photophysical properties of the synthesized dinuclear gold complexes, we next examined their photocatalytic performance. Specifically, we explored their application in direct dehalogenative three-component carbonylative amidation reactions under photochemical conditions. Notably, when employing $[Au_2dppm(dOMebpy)_2](OTf)_2$ (**4**) as the photocatalyst irradiated by 370 nm LEDs, the reaction between bromocyclohexane (**20**) and 1-(1-naphthyl)ethylamine (**21**) in DMSO under a CO atmosphere (balloon), with DMAP as an additive, afforded the target product (**22**) in 86% yield (Table 1, entry 1). Other dinuclear gold catalysts exhibited decreased reaction efficiency. The mononuclear gold complex[58] (**25**) was tested but proved catalytically inactive, underscoring the essential role of the dinuclear architecture in this transformation. Additionally, other commercially available photocatalysts, such as the strongly reducing *fac*-$Ir(ppy)_3$ (**26**), the strongly oxidizing $Ir[dF(CF_3)ppy]_2(dtbpy)]PF_6$ (**27**), and the organic photocatalyst 4-CzIPN (**28**), failed to promote the reaction. Control experiments further confirmed that the photocatalyst, additive, and light irradiation are all crucial for this three-component carbonylative amidation reaction (Table 1, entries 2-5).

Reaction mechanism study

A series of control experiments were carried out to gain insight into the mechanism of this gold-catalyzed three-component carbonylative amidation reaction. Screening different additives under standard conditions revealed that only DMAP was an efficient additive to promote this transformation (Fig. 4a). We speculated that an acyl pyridinium cation intermediate might be formed during the reaction[59]. To validate this hypothesis, the corresponding acyl pyridinium salt (**29**) was synthesized and reacted with primary amine (**21**) under standard conditions, which cleanly afforded the corresponding target product (**22**). This result supports the possible generation of acyl pyridinium intermediate in the catalytic cycle. Additional evidence for a radical pathway was obtained from radical inhibition experiments. The addition of TEMPO completely suppressed formation of product (**22**), and the corresponding cyclohexyl-TEMPO adduct was detected by HRMS, confirming a radical process (see Supplementary Information for details). Furthermore, addition of the spin-trap reagent *N*-tert-butyl-*α*-phenylnitrone (PBN) to the model reaction led to a strong radical signal in electron paramagnetic resonance (EPR) spectroscopy (Fig. 4b). Comparison with simulated spectra confirmed the signal originated from the PBN-trapped alkyl radical, with specific fitting

https://doi.org/10.1038/s41467-025-65926-2

Table 1 | Optimization of the reaction conditions[a]

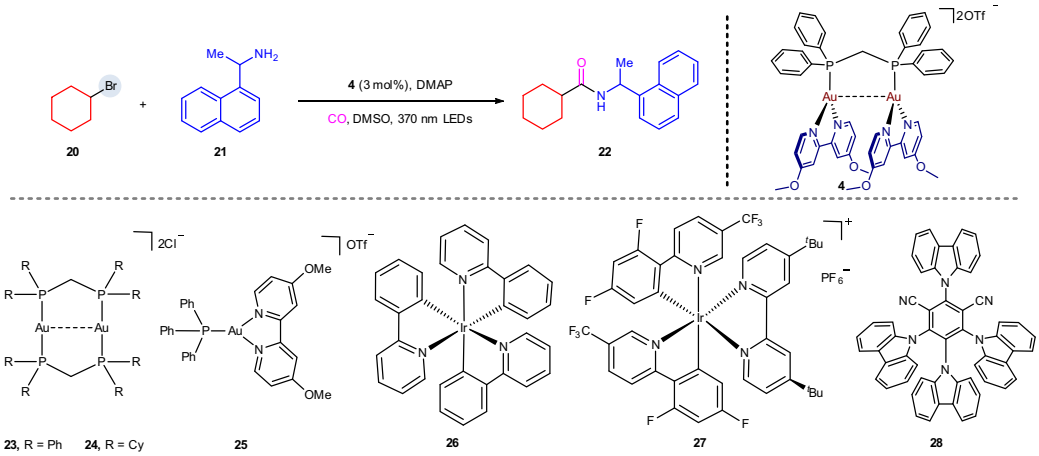

Entry	Variation of standard conditions	Yield [%][a]
1	none	86(84)[b]
2	without **4**	n.d.
3	without DMAP	trace
4	80 ºC (dark)	n.d.
5	with 3 mol% dppm or dOMebpy	n.d.

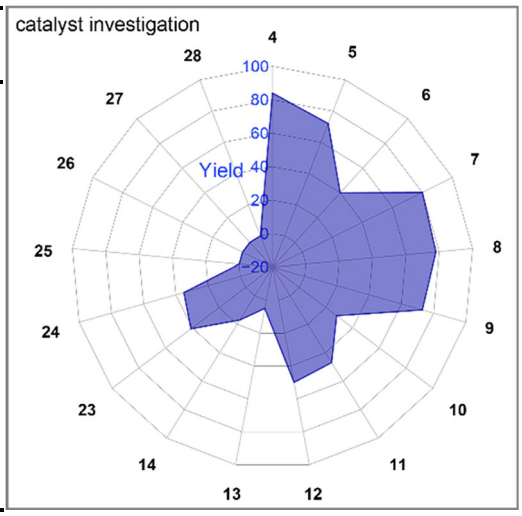

[a]Standard reaction conditions: **4** (3 mol%), **1a** (0.6 mmol), **2a** (0.2 mmol), DMAP (0.6 mmol), CO balloon, DMSO (1.0 mL), 370 nm LEDs, 12 h. [a] GC yield using dodecane as internal standard; [b] Isolated yield; n.d. = not detected. See details in Supplementary Information.

parameters of $g = 2.0062$, $a_N = 14.6$ G, and $a_H = 3.2$ G. Complementary evidence was provided by a radical clock experiment using 6-bromo-1-hexene (**30**) as the substrate, which exclusively afforded the cyclized product (**32**) under the standard conditions (Fig. 4c), further corroborating the presence of free radical intermediates.

Based on the experimental results, two plausible pathways were proposed for the three-component carbonylative amidation reaction (Fig. 4d). In path **A**, gold catalyst (**4**) undergoes photoexcitation to form its excited-state species **4***. Subsequent dynamic coordination of the alkyl bromide to photoexcited **4*** via the lone pair on the halogen atom leads to the formation of transition state **TS1**. This interaction facilitates an ISET process, resulting in the C-Br bond cleavage and formation of the cyclohexyl radical (**33**), along with the dinuclear gold species ($[Au_2Br^{2+}][OTf]_2$) (**34**). The resulting radical (**33**) then rapidly adds to CO, forming the acyl radical intermediate (**35**). In the presence of DMAP, the acyl radical adds to DMAP, yielding the zwitterionic radical intermediate (**36**). Subsequent SET oxidation of (**36**) by gold complex (**34**) produces the electrophilic alkylacyl-DMAP salt (**37**). This electrophilic intermediate then undergoes nucleophilic substitution with aniline (**21**) to afford amide product (**22**), concomitant with the regeneration of the ground-state gold catalyst. In path **B**, the acyl radical intermediate (**35**) is instead oxidized by the gold species (**34**) to form a highly reactive acylium cation (**38**). This intermediate subsequently is captured by the primary amine nucleophile (**21**) under DMAP assistance to afford the target product (**22**), regenerating the active gold catalyst and completing the catalytic cycle.

To gain a better insight into the reaction mechanism, density functional theory (DFT) calculations were conducted for the model reaction with **20** and **21** as substrates (Fig. 5, see details in Supplementary Information and Supplementary Data 1). Initially, the excited state of dinuclear gold complex $[Au_2dppm(dOMebpy)_2(OTf)_2]$ (**4***) undergoes an SET process with **20**, which results in the cleavage of C-Br bond and simultaneous generation of a cyclohexyl radical. Comparative analysis of different mechanistic pathways revealed that the ISET mechanism proceeds with a significantly lower activation barrier ($\Delta G^{\ddagger} = 19.0$ kcal mol^{-1}) than the outer-sphere SET (OSET) pathway, indicating a clear energetic preference for ISET[60–62]. The generated cyclohexyl radical subsequently undergoes carbonylation with CO and affords an acyl radical intermediate (**35**), which then reacts with DMAP to form a zwitterionic radical intermediate (**36**). The transition state energy barrier for this step is computed to be 14.3 kcal mol^{-1}. In contrast, direct generation of an acyl carbonium ion was found to require a free energy gain of 59.5 kcal mol^{-1}, rendering this pathway energetically prohibitive under the reaction conditions. Following the formation of intermediate (**36**), a subsequent SET oxidation by gold species (**34**) generates the acyl pyridinium cation (**37**) with a

https://doi.org/10.1038/s41467-025-65926-2

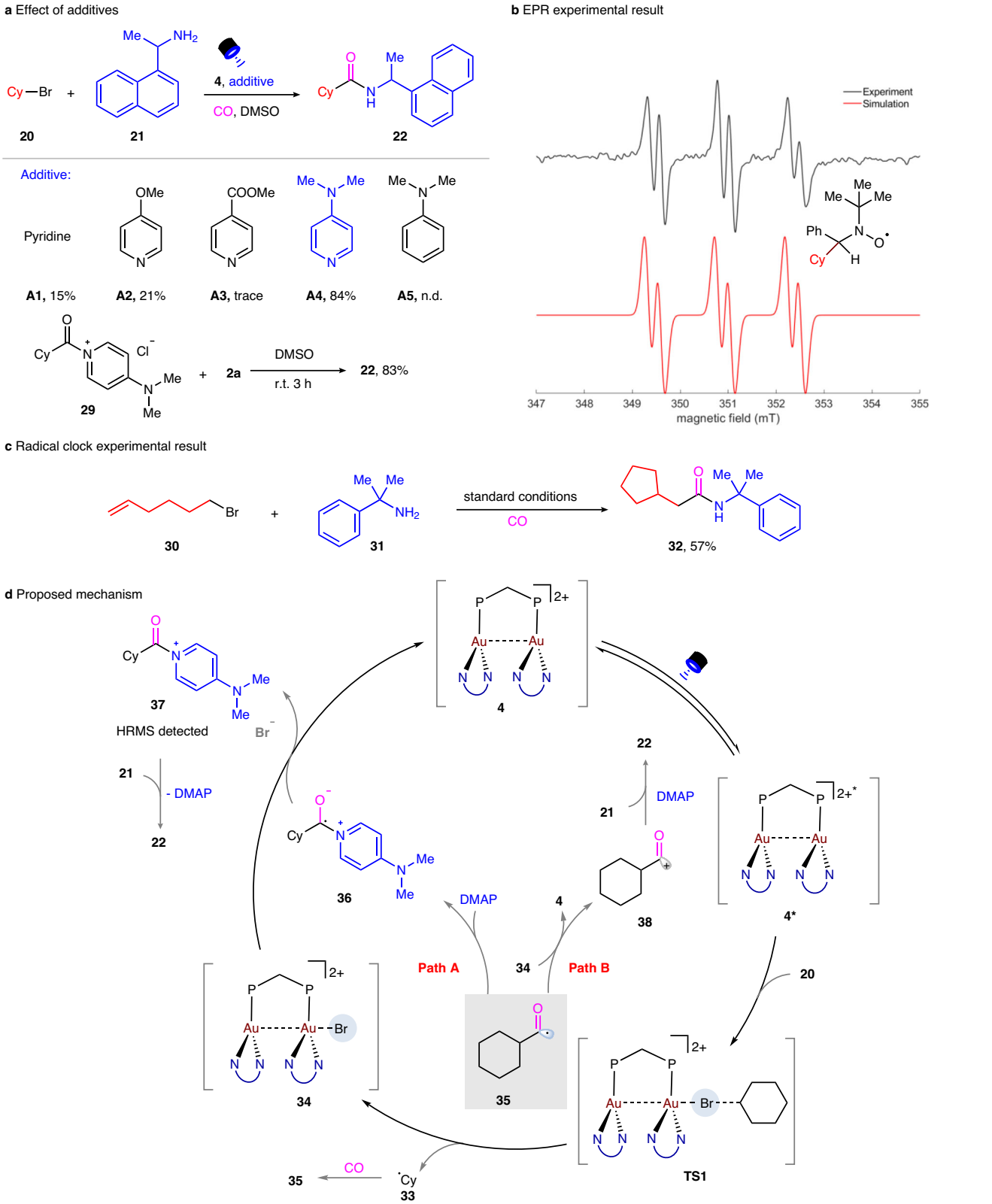

Fig. 4 | **Mechanism studies. a** Effect of additives. **b** EPR experimental result. **c** Radical clock experimental result. **d** Proposed mechanism.

low activation barrier ($\Delta G^{\ddagger} = 2.6$ kcal mol^{-1}). During this step, the bromine-containing dinuclear gold species (**34**) is reduced back to the original dinuclear gold catalyst. Ultimately, **37** undergoes nucleophilic substitution with **21**, affording the target product (**22**) and completing the catalytic cycle. To further investigate the distribution of unpaired electrons in the excited-state dinuclear gold complex during the reaction, spin density analyses were performed on the key intermediates (**4***, **INT1**, **TS1**, **INT2** and **34**). These results reveal a gradual electron transfer from the bidentate nitrogen ligands fragment to the metal center and alkyl halide substrate (**20**), which further confirms that the activation of alkyl halides would be promoted by the LLCT process of the dinuclear gold complex.

https://doi.org/10.1038/s41467-025-65926-2

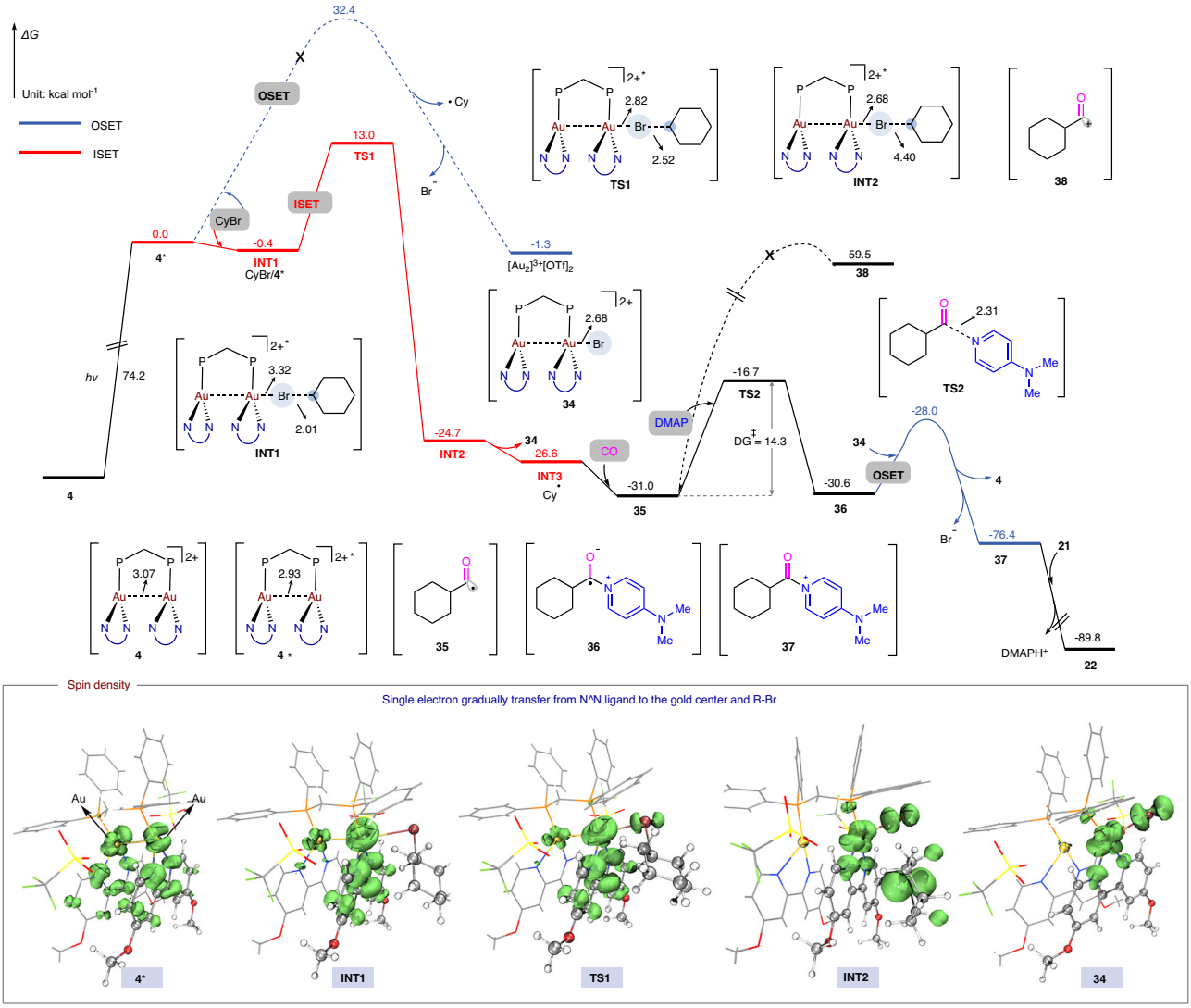

Fig. 5 | Computational studies about reaction mechanism. Free energy profiles calculated at the PBE(D3)/def2-SVP/def2-TZVP/CPCM(DMSO)//ωB97M-V/def2-TZVP/SMD(DMSO) level of theory. Isosurfaces for spin densities of selected structures are shown below (isovalue = 0.005).

Reaction substrate scope

Under the optimized reaction conditions, bromocyclohexane was selected as the starting material to explore the scope of amines in the three-component carbonylative amidation reaction (Fig. 6). The results indicated broad amine compatibility, with both aliphatic (primary and secondary) and aromatic amines proving to be competent coupling partners, affording the desired products in yields up to 96%. Notably, the transformation exhibited excellent functional group tolerance, as evidenced by successful incorporation of diverse functional groups such as ethers (**41**–**42**), cyano group (**43**), difluoromethyl (**54**), fluorine (**63**), and trifluoromethyl group (**67**). Furthermore, amines containing an internal olefin or terminal alkyne (**44**–**46**), as well as those bearing heterocyclic moieties (**50**–**52**) or steric hindered group (**56**), were well tolerated. This approach also exhibited good compatibility with sulfonamide substrate (**63**) and 2,2,2-trifluoroethylamine molecule (**64**). The late-stage functionalization of pharmaceutical molecules, including paroxetine (**65**), vortioxetine (**66**), desloratadine (**67**), dehydroabiethylamine (**68**), and fluoxetine (**69**), was successfully performed, affording the desired products with good yields ranging from 72% to 88%. We further explored the scope of arylamine substrates and found that a wide range of arylamines, bearing either electron-withdrawing or electron-donating groups, were well tolerated under the optimized reaction conditions. The corresponding amide products (**70**–**80**) were obtained in 41% to 82% yields.

As shown in Fig. 7, the protocol also exhibits broad applicability across primary, secondary, and tertiary bromoalkanes, delivering products (**81**–**98**) in moderate to good yields. It is worth mentioning that various active functional groups, such as silyl (**83**), fluoro (**84**), trifluoromethyl (**85**), chloro (**87**), ester (**88**), and boron compounds (**89**), were well tolerated. Additionally, cyclic secondary bromides bearing four to seven-membered rings proved to be competent substrates, giving rise to the desired products (**91**-**95**) in synthetically useful yields. For alkyl bromides containing heterocyclic structures (e.g., tetrahydropyran and piperidine), the reaction proceeded smoothly as well, providing products (**92**–**94**) with 58%-92% yields. Remarkably, even highly sterically hindered substrates afforded products (**96** and **97**) in 56% and 55% yields, respectively. Our investigation was further extended to hydroxyl molecules in this transformation. Notably, with 2-hydroxybenzyl alcohol (**99**) as substrate, the reaction tended to occur in the aliphatic hydroxyl group rather than the phenolic hydroxyl group. The phenolic hydroxyl group, despite its relatively lower nucleophilicity, participated smoothly in the transformation, producing the corresponding ester product (**102**) in 47% yield. Furthermore, simple 3-bromopropionic acid (**103**) was also tested, enabling the successful synthesis of sacubitril (**105**), an important therapeutic for chronic-heart-failure treatment[63].

https://doi.org/10.1038/s41467-025-65926-2

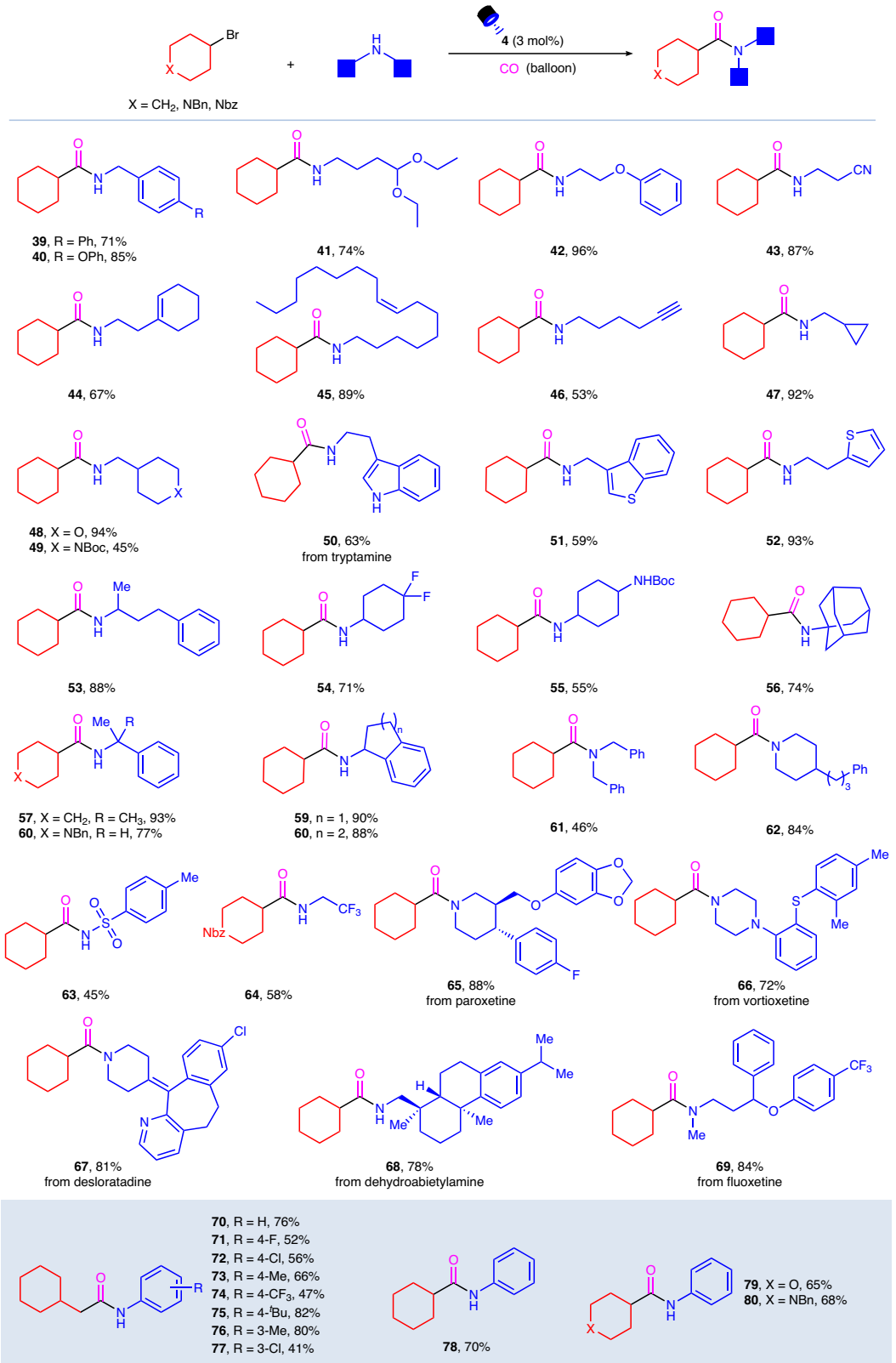

Fig. 6 | The substrate scope of amines. Reaction conditions: **4** (3 mol%), bromoalkanes (0.6 mmol, 3.0 equiv.), amines (0.2 mmol, 1.0 equiv), DMAP (0.6 mmol, 3.0 equiv.), CO balloon, DMSO (1.0 mL), 370 nm LEDs, 12 h.

Discussion

In summary, we have developed a bidentate mixed-ligand strategy for the construction of a class of dinuclear gold complexes, in which P^P- and N^N-type ligands coordinate to the gold centers. Interestingly, photophysical studies revealed that LLCT and Au–Au interactions play key roles in governing the excited-state behavior and catalytic performance of these complexes. Moreover, under mild conditions, these complexes have demonstrated excellent photoredox catalytic performance in selective three-component carbonylative amidation of unactivated alkyl halides with amines and CO (balloon). A wide range

https://doi.org/10.1038/s41467-025-65926-2

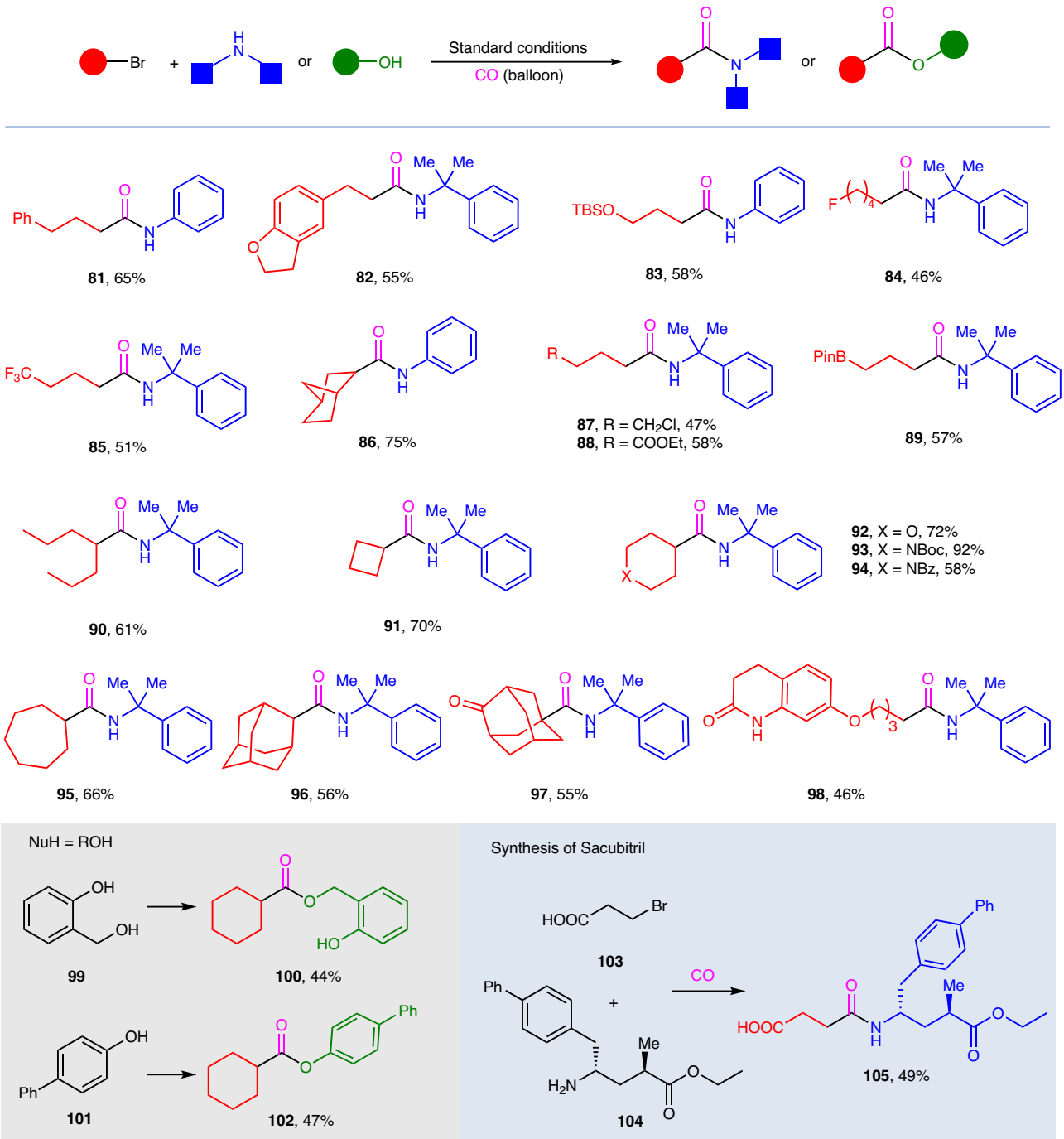

Fig. 7 | The substrate scope of alkyl bromides and other nucleophiles. Reaction conditions: **4** (3 mol%), bromoalkanes (0.6 mmol, 3.0 equiv.), nucleophiles (0.2 mmol, 1.0 equiv.), DMAP (0.6 mmol, 3.0 equiv.), CO balloon, DMSO (1.0 mL), 370 nm LEDs, 12 h.

of structurally diverse amides are produced in synthetically useful yields (64 examples, up to 96% yield). Mechanistic investigations uncovered a hybrid ISET/OSET pathway, in which the dinuclear gold catalyst facilitates both substrate activation and DMAP-assisted acyl pyridinium formation. These findings not only advance our fundamental understanding of gold photoredox catalysis, but also provide an avenue for the rational design of next-generation photocatalysts.

Methods

General procedure for synthesis of dinuclear gold-complex

To an oven-dried 10 mL sealed tube equipped with a magnetic stirring bar, **1** (1.0 equiv.) is added, followed by dry DCM. The tube is backfilled with argon. To this solution, the bipyridine ligand **2** (2.0 equiv.) and silver salt **3** (2.0 equiv.) are added, and the reaction mixture is stirred for 10 h. Afterward, celite is added, and the precipitate is filtered off. The solvent is concentrated, and the complex is precipitated with diethyl ether. Filtration and washing with diethyl ether afford dinuclear gold complexes **4**–**19** as a solid powder.

General procedure for three-component carbonylative amidation

To an oven-dried 10 mL sealed tube equipped with a magnetic stirring bar, 4 (3 mol%), bromoalkanes (0.6 mmol, 3.0 equiv.), amines (0.2 mmol, 1.0 equiv.), DMAP (0.6 mmol, 3.0 equiv., 73.2 mg) and

DMSO (1.0 mL) are added. The reaction mixture is degassed by three times backed with CO cycles and thenis vigorously stirred under the irradiation of 370 nm LEDs (distance ~4.0 cm from the bulb) for 12 h. After completion, the reaction mixture is removed from the light, diluted with water (10 mL), and extracted with ethyl acetate (5 mL) three times. The combined organic layers are washed with brine three times and dried over Na_2SO_4 and concentrated under reduced pressure. The residue is purified by silica gel chromatography (petroleum ether/ethyl acetate) to afford the corresponding desired product.

Data availability

Crystallographic data for the structures reported in this Article have been deposited at the Cambridge Crystallographic Data Centre, under deposition numbers CCDC 2403700 (**4**), CCDC 2403696 (**7**), CCDC 2403701 (**9**), CCDC 2403698 (**12**), and CCDC 2403702 (**25**). Copies of the data can be obtained free of charge via (https://www.ccdc.cam.ac.uk/structures/). Data related to materials and methods, optimization of conditions, experimental procedures, mechanistic experiments, and spectra are provided in the Supplementary information. Source data containing the coordinates of the optimized structures. All data are available from the corresponding authors upon request. Source data are provided with this paper.

References

1. Prier, C. K., Rankic, D. A. & MacMillan, D. W. C. Visible light photoredox catalysis with transition metal complexes: applications in organic synthesis. *Chem. Rev.* **113**, 5322–5363 (2013).
2. Cheung, K. P. S., Sarkar, S. & Gevorgyan, V. Visible light-induced transition metal catalysis. *Chem. Rev.* **122**, 1543–1625 (2022).
3. Cho, H., Tong, X., Zuccarello, G., Anderson, R. L. & Fu, G. C. Synthesis of tertiary alkyl amines via photoinduced copper-catalysed nucleophilic substitution. *Nat. Chem.* **17**, 271–278 (2025).
4. Hashmi, A. S. K. & Hutchings, G. J. Gold catalysis. *Angew. Chem. Int. Ed.* **45**, 7896–7936 (2006).
5. Chintawar, C. C., Yadav, A. K., Kumar, A., Sancheti, S. P. & Patil, N. T. Divergent gold catalysis: unlocking molecular diversity through catalyst control. *Chem. Rev.* **121**, 8478–8558 (2021).
6. Hendrich, C. M., Sekine, K., Koshikawa, T., Tanaka, K. & Hashmi, A. S. K. Homogeneous and heterogeneous gold catalysis for materials science. *Chem. Rev.* **121**, 9113–9163 (2021).
7. Hopkinson, M. N., Tlahuext-Aca, A. & Glorius, F. Merging visible light photoredox and gold catalysis. *Acc. Chem. Res.* **49**, 2261–2272 (2016).
8. Xia, Z. et al. Photosensitized oxidative addition to gold(i) enables alkynylative cyclization of o-alkylnylphenols with iodoalkynes. *Nat. Chem.* **11**, 797–805 (2019).
9. Wu, J. et al. Photosensitized Gold-Catalyzed Cross-Couplings of Aryl Bromides. *J. Am. Chem. Soc.* **147**, 5839–5850 (2025).
10. Liu, K., Li, N., Ning, Y., Zhu, C. & Xie, J. Gold-catalyzed oxidative biaryl cross-coupling of organometallics. *Chem* **5**, 2718–2730 (2019).
11. Liu, D.-Y. et al. Dinuclear Gold-Catalyzed para-selective C-H arylation of undirected arenes by noncovalent interactions. *Angew. Chem. Int. Ed.* **62**, e202313122 (2023).
12. Liang, H., Julaiti, Y., Zhao, C.-G. & Xie, J. Electrochemical gold-catalysed biocompatible C(sp2)–C(sp) coupling. *Nat. Synth.* **2**, 338–347 (2023).
13. Fang, S. et al. Cooperative dinuclear gold catalysis unlocking 1,2-reductive elimination elementary reaction in oxidative C—C coupling. *Angew. Chem. Int. Ed.* **64**, e202506925 (2025).
14. Liu, D.-Y. et al. Gold and bismuth trimetallic synergistic redox catalysis for non-directed C—H arylation with aryl bismuth. *Angew. Chem. Int. Ed.* **64**, e202510357 (2025).
15. Che, C.-M., Kwong, H.-L., Yam, V. W.-W. & Cho, K.-C. Spectroscopic properties and redox chemistry of the phosphorescent excited state of $[Au_2(dppm)_2]^{2+}$[dppm = bis(diphenylphosphino)methane]. *J. Chem. Soc. Chem. Commun.* **13**, 885–886 (1989).
16. Li, D., Che, C.-M., Kwong, H.-L. & Yam, V. W.-W. Photoinduced C–C bond formation from alkyl halides catalysed by luminescent dinuclear gold(I) and copper(I) complexes. *J. Chem. Soc. Dalton trans.* **23**, 3325–3329 (1992).
17. Revol, G., McCallum, T., Morin, M., Gagosz, F. & Barriault, L. Photoredox transformations with dimeric gold complexes. *Angew. Chem. Int. Ed.* **52**, 13342–13345 (2013).
18. McCallum, T. & Barriault, L. Direct alkylation of heteroarenes with unactivated bromoalkanes using photoredox gold catalysis. *Chem. Sci.* **7**, 4754–4758 (2016).
19. Zhang, L. et al. Reductive C–C coupling by desulfurizing gold-catalyzed photoreactions. *ACS Catal.* **9**, 6118–6123 (2019).
20. Zhang, L., Si, X., Rominger, F. & Hashmi, A. S. K. Visible-light-induced radical carbo-cyclization/gem-diborylation through triplet energy transfer between a gold catalyst and aryl iodides. *J. Am. Chem. Soc.* **142**, 10485–10493 (2020).
21. Zhao, Y. et al. Gold catalysed site-selective cross-coupling of tertiary α-silylamines with 1-iodoalkynes under UVA LED light. *Org. Chem. Front.* **10**, 759–766 (2023).
22. Ji, C.-L. et al. Photoinduced gold-catalyzed divergent dechloroalkylation of gem-dichloroalkanes. *Nat. Catal.* **5**, 1098–1109 (2022).
23. Han, J. et al. Photoinduced manganese-catalysed hydrofluorocarbofunctionalization of alkenes. *Nat. Synth.* **1**, 475–486 (2022).
24. Fang, Q.-Y. et al. Trinuclear gold-catalyzed 1,2-difunctionalization of alkenes. *Angew. Chem. Int. Ed.* **62**, e202305121 (2023).
25. Pang, Y. et al. Dimeric manganese-catalyzed hydroalkenylation of alkynes with a versatile silicon-based directing group. *Angew. Chem. Int. Ed.* **62**, e202306922 (2023).
26. Xia, S. et al. Gold–manganese bimetallic redox coupling with light. *J. Am. Chem. Soc.* **145**, 26756–26764 (2023).
27. Ji, C.-L. et al. Dinuclear gold-catalyzed divergent dechlorinative radical borylation of gem-dichloroalkanes. *Nat. Commun.* **15**, 3721 (2024).
28. Fang, Q.-Y. et al. Trinuclear gold-catalyzed site-selective alkylation of peptides. *Sci. China Chem.* **68**, 249–256 (2025).
29. Chen, K. et al. Switch in selectivities by dinuclear nickel catalysis: 1,4-hydroarylation of 1,3-dienes to z-olefins. *J. Am. Chem. Soc.* **145**, 24877–24888 (2023).
30. Shao, L. et al. Enantioselective construction of cyclic quaternary stereocenters via dinuclear copper catalyzed asymmetric [3 + 2] propargylation/annulation. *Nat. Commun.* **16**, 7191–7201 (2025).
31. Lu, Y.-L., Lan, W.-L., Shi, W., Jin, Q.-H. & Cheng, P. Photo-induced variation of magnetism in coordination polymers with ligand-based electron transfer. *Dalton Trans.* **50**, 13124–13137 (2021).
32. Huo, P. et al. Ligand-to-ligand charge transfer within metal–organic frameworks based on manganese coordination polymers with tetrathiafulvalene-bicarboxylate and bipyridine ligands. *Inorg. Chem.* **55**, 6496–6503 (2016).
33. Zhang, C., Tang, C. & Jiao, N. Recent advances in copper-catalyzed dehydrogenative functionalization via a single electron transfer (SET) process. *Chem. Soc. Rev.* **41**, 3464–3484 (2012).
34. Han, J. & Xie, J. Inner-sphere single electron transfer in polynuclear gold photocatalysis. *ChemCatChem* **15**, e202300974 (2023).
35. Huang, J. et al. Photoinduced copper-catalyzed C–N coupling with trifluoromethylated arenes. *Nat. Commun.* **14**, 8292 (2023).
36. Peng, J.-B., Wu, F.-P. & Wu, X.-F. First-row transition-metal-catalyzed carbonylative transformations of carbon electrophiles. *Chem. Rev.* **119**, 2090–2127 (2019).
37. Tien, C.-H. et al. Carboxyboronate as a versatile in situ CO surrogate in palladium-catalyzed carbonylative transformations. *Angew. Chem. Int. Ed.* **60**, 4342–4349 (2021).
38. Forni, J. A., Micic, N., Connell, T. U., Weragoda, G. & Polyzos, A. Tandem photoredox catalysis: enabling carbonylative amidation

of aryl and alkylhalides. *Angew. Chem. Int. Ed.* **59**, 18646–18654 (2020).
39. Li, L., Hu, Z., Ren, S., Arndtsen, B. A. & Chu, L. Enantioselective carbonylative coupling reactions: merging nickel-based selectivity and photoredox reactivity. *J. Am. Chem. Soc.* **147**, 28206–28214 (2025).
40. Kuai, C.-S., Yuan, Y. & Wu, X.-F. Emerging trends in CO carbonylation. *Chem* **11**, 102503 (2025).
41. Zhao, F., Ai, H.-J. & Wu, X.-F. Copper-catalyzed substrate-controlled carbonylative synthesis of α-keto amides and amides from alkyl halides. *Angew. Chem. Int. Ed.* **61**, e202200062 (2022).
42. Wang, J. et al. Synchronous recognition of amines in oxidative carbonylation toward unsymmetrical ureas. *Science* **386**, 776–782 (2024).
43. Cao, Y. & He, L. Synthesis of carbonyl compounds by gold-catalyzed carbonylation reactions. *Synlett* **33**, 1003–1010 (2022).
44. Ahrens, A. et al. Experimental and theoretical studies on gold(III) carbonyl complexes: reductive C,H- and C,C bond formation. *Dalton Trans.* **50**, 8752–8760 (2021).
45. Akram, M. O., Banerjee, S., Saswade, S. S., Bedi, V. & Patil, N. T. Oxidant-free oxidative gold catalysis: the new paradigm in cross-coupling reactions. *Chem. Commun.* **54**, 11069–11083 (2018).
46. Bhoyare, V. W., Bera, A., Gandon, V. & Patil, N. T. Gold-catalyzed alkoxy-carbonylation of aryl and vinyl iodides. *Angew. Chem. Int. Ed.* **63**, e202410794 (2024).
47. Peng, H. et al. Gold-Catalyzed Oxidative Cross-Coupling of Terminal Alkynes: Selective Synthesis of Unsymmetrical 1,3-Diynes. *J. Am. Chem. Soc.* **136**, 13174–13177 (2014).
48. Cai, R. et al. Ligand-assisted gold-catalyzed cross-coupling with aryldiazonium salts: redox gold catalysis without an external oxidant. *Angew. Chem. Int. Ed.* **54**, 8772–8776 (2015).
49. Ye, X. et al. Facilitating gold redox catalysis with electrochemistry: an efficient chemical-oxidant-free approach. *Angew. Chem. Int. Ed.* **58**, 17226–17230 (2019).
50. Shi, H. et al. Bidentate N-ligand-assisted gold redox catalysis with hydrogen peroxide. *Nat. Chem.* **17**, 822–834 (2025).
51. Iwai, T., Abe, S., Takizawa, S. -y, Masai, H. & Terao, J. Insulated π-conjugated 2,2′-bipyridine transition-metal complexes: enhanced photoproperties in luminescence and catalysis. *Chem. Sci.* **15**, 8873–8879 (2024).
52. Verma, C. et al. Coordination complexes of bipyridines (CCBs): chemistry, bonding and applications. *Coord. Chem. Rev.* **529**, 216433–216490 (2025).
53. Yang, Y. et al. Trans influence of ligands on the oxidation of gold(I) complexes. *J. Am. Chem. Soc.* **141**, 17414–17420 (2019).
54. Luong, L. M. C. et al. Unsymmetrical coordination of bipyridine in three-coordinate gold(I) complexes. *Inorg. Chem.* **59**, 4109–4117 (2020).
55. Lu, T. & Chen, F. W. Multiwfn: A multifunctional wavefunction analyzer. *J. Comput. Chem.* **33**, 580–592 (2012).
56. Liu, Z., Lu, T. & Chen, Q. An sp-hybridized all-carboatomic ring, cyclo[18]carbon: electronic structure, electronic spectrum, and optical nonlinearity. *Carbon* **165**, 461–467 (2020).
57. Lu, T. A comprehensive electron wavefunction analysis toolbox for chemists, Multiwfn. *J. Chem. Phys.* **161**, 82503–82545 (2024).
58. Shmelev, N. Y. et al. Asymmetric coordination mode of phenanthroline-like ligands in gold(I) complexes: A Case of the Antichelate Effect. *Cryst. Growth Des.* **22**, 3882–3895 (2022).
59. Xu, S. et al. The DMAP-catalyzed acetylation of alcohols—a mechanistic study (DMAP=4-(dimethylamino)pyridine). *Chem. Eur. J.* **11**, 4751–4757 (2005).
60. Marcus, R. A. On the theory of oxidation-reduction reactions involving electron transfer. I. *J. Chem. Phys.* **24**, 966–978 (1956).
61. Ren, H. et al. How does iridium(iii) photocatalyst regulate nickel(ii) catalyst in metallaphotoredox-catalyzed C–S cross-coupling? Theoretical and experimental insights. *ACS Catal.* **9**, 3858–3865 (2019).
62. Truhlar, D. G., Garrett, B. C. & Klippenstein, S. J. Current status of transition-state theory. *J. Phys. Chem.* **100**, 12771–12800 (1996).
63. Feldman, A. M., Haller, J. A. & DeKosky, S. T. Valsartan/sacubitril for heart failure: reconciling disparities between preclinical and clinical investigations. *JAMA* **315**, 25–26 (2016).

Acknowledgements

We thank National Natural Science Foundation of China (22471121, 22471122, 22271144), National Key Research and Development Program of China (2022YFA1500), Fundamental Research Funds for the Central Universities (020514380327) and the Open Project of State Key Laboratory of Natural Medicines (SKLNMKF202401) for financial support. All theoretical calculations were performed at the High-Performance Computing Center (HPCC) of Nanjing University. Junheng Liu and Yulan Chen at Nanjing University for reproduction of the experimental procedures for products **42** and **91**.

Author contributions

J.X. conceived the work and designed the experiments. Q.F., S.X., T.L., Y.G., X.W. and performed the experiments and analyzed the experimental data. Q.F. performed the density functional theory calculations and discussed the results with J.H. Q.F., W.L., C.Z. and J.X. co-wrote the manuscript with the input from all the other authors.

Competing interests

The authors declare no competing interests.

Additional information

Supplementary information The online version contains supplementary material available at https://doi.org/10.1038/s41467-025-65926-2.

Correspondence and requests for materials should be addressed to Xiaopeng Wu, Weipeng Li, Chengjian Zhu or Jin Xie.

Peer review information *Nature Communications* thanks Zhonghua Xia, and the other, anonymous, reviewers for their contribution to the peer review of this work. A peer review file is available.